RPE | Radiation Physics & Engineering
A Peer-Reviewed Journal
Published by K.N. Toosi University of Technology
http://rpe.kntu.ac.ir
Research Article

Radiation Physics and Engineering 2026; 7(3):75–88

Bi_2O_3/silicone rubber composite thyroid shield in periapical radiography: Experimental and Monte Carlo assessment

Shahryar Malekie[a,*], Leila Shahbazi[b], Dariush Sardari[c], Sedigheh Kashian[a], Mohsen Kheradmand Saadi[d]

[a] *Radiation Application Research School, Nuclear Science and Technology Research Institute (NSTRI), P.O. Box 3148643111, Karaj, Iran*
[b] *Tehran University of Medical Sciences, Tehran, Iran*
[c] *Department of Medical Radiation Engineering SR.C., Islamic Azad University, Tehran, Iran*
[d] *Department of Nuclear Engineering, SR.C., Islamic Azad University, Tehran, Iran*

HIGHLIGHTS

- Bi_2O_3/SR composite thyroid collar (4 mm thick, 70 wt% Bi_2O_3) for periapical radiography.
- Composite (mass thickness 1.072 g.cm^{-2}) vs. commercial shield (0.5 mm Pb equivalent, mass thickness 0.714 g.cm^{-2}).
- TLD-GR200 measurements in Rando phantom: 71.4% thyroid dose reduction (composite) vs. 43.7% (commercial).
- MCNP simulation at 60°: 85.1% dose reduction (commercial) vs. 83.3% (composite).
- Superior shielding performance under broad-beam conditions (99.97% vs. 99.08% air kerma reduction).

ABSTRACT

A thyroid shield composed of 70 wt% micro-sized Bi_2O_3 dispersed in a silicone rubber matrix was evaluated for radiation protection efficacy in periapical dental radiography. Absorbed dose to the thyroid gland was quantified using both Monte Carlo N-Particle (MCNP) simulations with a modified MIRD phantom and experimental measurements employing TLD-GR200 dosimeters positioned in the superior and inferior thyroid regions of a Rando anthropomorphic phantom. Irradiations were performed at 60 kV, 7 mA, and 0.32 s exposure time with a fixed 60° vertical angulation. Experimental results revealed thyroid absorbed doses of 72.7±25.7 μGy (unshielded), 40.9±15.6 μGy (commercial collar equivalent to 0.5 mm Pb), and 20.8±12.5 μGy (composite shield), corresponding to a 71.4% dose reduction with the composite shield, (compared to 43.7% for the commercial collar). Monte Carlo simulations at 60° angulation demonstrated dose reductions of 85.1% (commercial), and 83.3% (composite). Additionally, under SSDL inverse broad-beam conditions based on the IEC 61331-1 (RQR5, 70 kV), the composite shield achieved a 99.97% air kerma rate reduction, markedly superior to the 99.08% (commercial) and 98.13% (0.5 mm pure Pb). Although the composite shield exhibited superior shielding performance, its weight remains higher than commercial alternatives, indicating the need for further optimization.

KEYWORDS

Thyroid shield
Bi_2O_3/SR composite
Dental periapical
Rando phantom
MCNP code

HISTORY

Received: 15 February 2026
Revised: 20 June 2026
Accepted: 27 June 2026
Published: Summer 2026

1 Introduction

Dental radiography, a critical diagnostic tool, enables the visualization of teeth and surrounding structures to identify oral pathologies and injuries. Dental radiography is the dominant imaging method utilized in dentistry, as stated in the 2010 report by the United Nations Scientific Committee on the Effects of Atomic Radiation (UNSCEAR), and it remains essential in everyday dental practice (Charles, 2010). Among the three dental radiography methods, which consist of Cone Beam Computed Tomography (CBCT), panoramic imaging through Orthopantomogram (OPG), and periapical radiography, the CBCT technique is specifically designed for diagnostic and specialized purposes. On the other hand, panoramic and periapical radiographs are the most widely employed methods (Aghaz et al., 2021, 2018).

Interaction of radiation with matter plays an important role to assess the shielding properties of a material

*Corresponding author: smaleki@aeoi.org.ir

https://doi.org/10.22034/rpe.2026.575950.1344

(Al-Buriahi et al., 2021; Ufuk et al., 2016; Urtekin et al., 2020; Demir et al., 2019). In the healthcare sector, radiation protection devices are commonly placed in direct contact with the human body to reduce radiation exposure to radiosensitive organs during diagnostic and interventional X-ray procedures. Research has linked dental radiography to potential health risks, including an elevated incidence of thyroid cancer, genotoxic effects in pediatric patients, and the development of salivary gland and intracranial tumors. Thus, in dentistry, the diagnostic radiographic doses should be maintained at levels of as low as reasonably achievable (ALARA), while still ensuring adequate image quality and protecting radiosensitive organs. Periapical or Intra-oral radiography, in particular, is one of the most significant and commonly used diagnostic methods for a variety of dental pathologies to provide detailed images of individual teeth, their roots, and adjacent bone, facilitating the detection of conditions such as periapical lesions and root fractures (Nair and Nair, 2007; Janani et al., 2021; Mishra et al., 2018). Studies report that periapical radiography delivers effective doses ranging from 5-20 μSv, depending on equipment and technique (Ludlow et al., 2008).

The thyroid gland, a vital endocrine organ located anteriorly in the neck and weighing approximately 15-20 grams, regulates metabolism and growth through hormone production (Ufuk et al., 2016; Urtekin et al., 2020). The National Council on Radiation Protection and Measurements (NCRP report No. 145) (National Council on Radiation Protection and Measurements, 2003), advocates for the implementation of thyroid shielding in pediatric patients and suggests that such shielding should also be applied to adults, provided it does not interfere with the examination. Also, The NCRP No. 145 recommends various strategies to reduce radiation exposure in dental practices, including implementation of rectangular collimation for all Intra-oral imaging, the utilization of rapid image receptors, the maintenance of a minimum source-to-skin distance of 20 cm, and the application of selection criteria to ascertain the necessity of radiographic examinations.

To reduce radiation exposure, it is advisable to use thyroid collars, lead aprons, lead glasses, and bismuth shielding to safeguard radiosensitive organs located within or near the scanning area. Specifically, thyroid shields have been shown to achieve dose reductions up to 75% to the thyroid gland when used properly (Kim et al., 2010). Commercially, bismuth shielding is available in different thicknesses, and a thickness of 1 mm is considered to have a lead equivalent of 0.06 mm (Vollmar and Kalender, 2008; Einstein et al., 2012). Conventional lead-based thyroid shields, while effective, pose challenges due to lead's toxicity, which can cause neurological damage, anemia, and environmental harm due to its non-recyclable nature. These concerns have prompted research into lead-free alternatives. Previous studies by the authors explored polymer-heavy metal oxide nanocomposites with high surface-to-volume ratio nanoparticles as innovative radiation shields for nuclear medicine and diagnostic imaging (Mehrara et al., 2021; Malekie et al., 2022; Hosseini et al., 2022; Jayakumar et al., 2023). Recent advancements highlight polymer composites as viable radiation shielding materials across various energy levels (Srinivasan and Samuel, 2017; More et al., 2021; Gholamzadeh et al., 2020; Aghaz et al., 2016; Mortazavi et al., 2013; Demirel and Ycel, 2024). However, they are not employed in OPG as they might hinder the primary beam, and additional research is needed concerning their application in CBCT (Kelaranta et al., 2016). Numerous studies have been conducted on the design and fabrication of thyroid shields. For example, recently, Takegami et al. developed an innovative thyroid shield with reduced artifacts to address issues concerning image quality. The shield incorporated fine bismuth oxide particles embedded within low-density polyurethane (PU) foam (Takegami et al., 2023). Bawazeer et al., evaluated the impact of a commercial thyroid shield utilized in OPG, and CBCT (Bawazeer et al., 2024).

At the previous study by the authors, a flexible thyroid shield based on the Bi_2O_3/SR composite was evaluated in dental panoramic radiography (OPG model Orthopantomograph OP200D, 75 kV, 13 mA, and exposure time of 14.1 s) (Shahbazi et al., 2026). The present study extends this investigation to periapical (Intra-oral) radiography, a more frequently performed procedure with different beam geometry and scatter characteristics, demonstrating the composites performance under clinically conditions (Shahbazi et al., 2026). To achieve this objective, the study was conducted in two phases. In the experimental phase, TLD-GR200 dosimeters were placed within the thyroid region of an adult male Rando anthropomorphic phantom, with the X-ray tube angle fixed at 60°. Furthermore, to assess and compare the protective efficacy of the composite shield with a commercial thyroid protector in accordance with the IEC 61331 standard method (IEC 61331-1, 2014; IEC 61331-3, 2014; Eder and Schlattl, 2018), measurements were performed using the broad-beam technique at the Secondary Standards Dosimetry Laboratory (SSDL) of Iran. In the simulation phase, the Monte Carlo N-Particle (MCNP) code was employed to calculate the absorbed dose to the thyroid gland at various tube angles.

2 Materials and methods

2.1 Design and fabrication of the composite shield

The composite shield design based on the standard model (33, 2024), is illustrated in Fig. 1. The thickness of the fabricated composite was considered as 4 mm, near to Tenth Value Layer (TVL) amount of the composite as 3.1 mm based on the online XCOM and previous work (Shahbazi et al., 2026; Berger and Hubbell, 1987), to achieve effective attenuation while maintaining flexibility. The detailed procedure for the fabrication of Bi_2O_3/silicone rubber composites has been previously reported by the authors (Shahbazi et al., 2026); therefore, only a brief description is provided here. A Bi_2O_3/silicone rubber composite (70 wt% Bi_2O_3) was made by mixing and ultrasonication, curing with a hardener, and molding. It was post-cured to create a flexible 4 mm thyroid shield with a density of 2.68 g.cm^{-3} (Shahbazi et al., 2026).

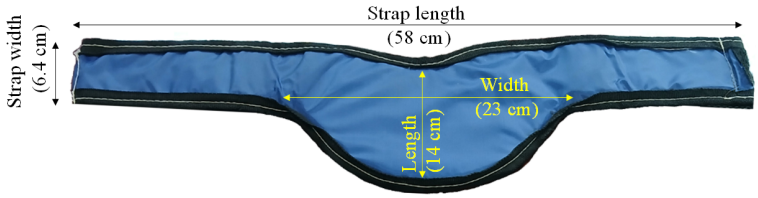

Figure 1: Exhibition of dimensional attributes of the composite shield, with thickness of 4 mm.

(a) (b) (c)

Figure 2: Experimental setup of the irradiation the phantom at periapical position with angle of 60, (a) without shield, (b) composite shield (this work), and (c) lead shield.

Table 1: Comparison of the mass thickness, and dimensions for commercial and composite shields.

Thyroid shield	Thickness (mm)	Density ($g.cm^{-3}$)	Mass thickness ($g.cm^{-2}$)	Effective area (cm^2)	Weight (g)
Composite (70 wt% Bi_2O_3/SR)	4	2.68	1.072	∼500	∼600
Commercial shield equivalent to 0.5 mm Pb	1.7	4.2	0.714	∼500	∼400

Table 1 presents data on the mass thickness, and dimensions for two products: commercial and micro composite-based thyroid shields, both of which share identical shapes. It is important to note that the weight values listed in Table 1 include the waterproof fabric that surrounds each shield. As can be seen from Table 1, the mass thickness (thickness×nominal density) is provided for comparative purposes with the measured physical properties of the composite shield. Also, the ratio of areal densities between the composite and commercial shields corresponds precisely to their weight ratio.

2.2 Instruments for irradiation and measurements

Periapical radiography was conducted utilizing the CS 2100 unit along with an RVG digital sensor from Carestream Dental, LLC, operating at 60 kV, and 7 mA. The exposure time was established at 0.32 s, resulting in a measured dose of approximately 1.95 mGy (with accuracy of ±30%) at the end of a standard cone with 20 cm length, and diameter of 6 cm, with an exposure surface of 28.3 cm2. The angle of central irradiation was adjusted to 60°. The CS 2100 unit comprises several key components: a high-frequency X-ray generator that includes transformer and related electronics, as well as an oil-cooled X-ray tube. Additionally, it features a beam-limiting device characterized by a radiation diameter of 6 cm and a distance of 20 cm from the focal spot of the X-ray tube to the skin.

In Fig. 2, the setup of irradiation for a periapical device is exhibited at three positions, namely without shield or unshielded, composite shield, and a conventional lead thyroid. A collection of calibrated TLD-GR200 dosimeters (LiF: Mg, Cu, P), featuring a thickness of 0.9 mm and a diameter of 4 mm, was utilized with a Harshaw 4500 TLD Reader. All readings and annealing processes of the TLDs were conducted at the NSTRI in Tehran, Iran.

However, in periapical dental radiography, thyroid exposure originates predominantly from scattered radiation generated within the patients head and neck tissues, with minimal primary beam contribution. Our phantom-based broad-beam experiment (6 cm field, 20 cm SSD, 60° angulation) is designed to assess clinically significant protection under realistic conditions, where the shield is required to attenuate both primary and scattered photons that reach the gland. Based on prior measurements of the 70 wt% Bi_2O_3/silicone rubber composite shield in OPG radiography using a Rando phantom, the recorded 71.4% dose reduction to the thyroid demonstrates a genuine patient benefit that narrow-beam tests alone cannot reflect. Complementary narrow-beam validation for this composite was previously performed at Iran's SSDL (Shahbazi et al., 2026).

In this study, to evaluate the effectiveness of the composite thyroid shield in radiation protection, a head-neck section of an adult male Rando phantom (Serial number

Table 2: Calibration factors of TLDs GR-200 for 60 kV related to periapical radiography.

Radiation quality	Mean energy (keV)	$Hp(10)/K_a$	N_k (μSv.nC^{-1})	Reference
X-rays (60 kV)	48	1.65	3.01	(IAEA, 2018)
Co-60	1250	1.15	2.1	Experiment, this work

759) was utilized (see Fig. 2), with the shield positioned around the neck of the phantom. It is important to highlight that the thyroid gland in the Rando phantom is situated within slices #9 and #10 (Shahbazi et al., 2026). The slice thickness is standardized as 25 mm. Standard Rando phantoms are generally constructed from tissue-equivalent materials (e.g., a mix simulating soft tissue, bone, and lungs with specific densities). This specific anatomical arrangement facilitates a clear assessment of both the upper and lower portions of the thyroid during the experimental analysis entitled as superior, and inferior positions, respectively (Shahbazi et al., 2026). To quantify the radiation dose received by the thyroid gland, the TLD dosimeters were strategically placed at eight locations on slices #9, and #10, specifically at the center, right, left, and anterior parts of the thyroid (with four TLDs allocated to each slice). Ultimately, the average dose across these various sites was taken as the representative dose for the thyroid gland. It should be mentioned that due to the larger diameter of the TLD dosimeters (4 mm) relative to the embedded holes in the Rando phantom, accurate positioning within the designated locations was not feasible. Consequently, the dosimeters were placed on the surfaces of the phantom slices. This placement may increase uncertainty in estimating the absorbed dose to the thyroid gland.

The amount of dose in each TLD dosimeter can be obtained as (Shahbazi et al., 2026):

$$\text{Dose } (\mu\text{Sv}) = N_k \ (\mu\text{Sv.nC}^{-1}) \times [Q - Q_b](\text{nC}) \times \left(\frac{Rl_0}{Rl_1}\right) \quad (1)$$

where N_k is the calibration factor of the TLD-GR200 dosimeter (in μSv.nC^{-1}), determined experimentally and adjusted for the X-ray energy spectrum as is described in Section 2.3, Q represents the intensity or electric charge of the dosimeters measured in nC, while Q_b indicates the background dose reading. A crucial aspect to note is that, given that two TLDs are utilized as controls, it is necessary to subtract the background dose from each individual reading. Additionally, an Element Correction Coefficient (ECC) is applied to refine the readings of each dosimeter, thereby ensuring the accuracy of the resultant dose measurement. More specifically, the ECC for a particular dosimeter (denoted as ECC$_i$) is defined as the ratio of the average reading from the group of TLDs, represented as $\langle \text{TLD} \rangle$, to the reading recorded by that specific TLD dosimeter namely TLD$_i$ (Moafi et al., 2015):

$$ECC_i = \frac{\langle TLD \rangle}{TLD_i} \quad (2)$$

The additional correction factor in Eq. (1) is the reference level ratio, denoted as $\left(\frac{Rl_0}{Rl_1}\right)$, which is attributed to the stability of the reader and is recorded for every ten measurements.

Before the irradiation process, it is significant to mention that the TLD dosimeters were subjected to an annealing procedure in an oven at 240 °C for a duration of 10 minutes. This annealing step was carried out twice, with each session lasting for 10 minutes. Following the irradiation, the TLDs were exposed to a preheating phase in an oven maintained at 100 °C for 10 minutes before being read by the TLD reader. Finally, the dose reduction can be assessed as (Lee et al., 2011):

$$\text{Dose reduction } (\%) = \left(\frac{\text{unshielded dose - shielded dose}}{\text{unshielded dose}}\right) \times 100 \quad (3)$$

2.3 Calibration of the dosimeters

The responses of TLD GR-200 dosimeters were calibrated at the SSDL of Iran, against the gamma-rays of Co-60. The calibration factor (N_k) was obtained as 2.1 μSv.nC^{-1} using a PMMA phantom for Co-60 at the SSDL of Iran. Based on the reference (Hafezi et al., 2018), $Hp(10)$[Sv]= $f.k_a$[Gy], in which f or $Hp(10)/K_a$ is conversion coefficient of air kerma (k_a) to personal dose equivalent, namely $Hp(10)$. For Co-60, N_k = 2.1 (μSv.nC^{-1}), and $f = Hp(10)/K_a = 1.15$, thus $K_a = Hp(10)/f$. For X-rays 60 kV, with mean energy of 48 keV, $f = 1.65$ (Hafezi et al., 2018), thus N_k can be obtained as (2.1 μSv.nC^{-1} $\times$1.65)/1.15=3.01 μSv.nC^{-1}. The details of obtaining the calibration factor of TLDs for X-rays at 60 kV related to periapical radiography is exhibited in Table 2. It is important to note that 60Co serves as a standard for calibrating the TLDs used in X-ray applications within dental radiology (Qu et al., 2012).

Determination of calibration factor in Eq. (1), namely N_k, plays an important role in dosimetry process. Calibration factor of a TLD dosimeter can be obtained for X-ray field at a specified energy (mean energy) using the Co-60 as reference field (Attix, 2008):

$$N_k \ (\mu\text{Sv.nC}^{-1})|_{\overline{E}_{(X-ray)}} \cong N_k \ (\mu\text{Sv.nC}^{-1})|_{ref} \times \frac{\left[\frac{(\mu_{en}/\rho)_{LiF}}{(\mu_{en}/\rho)_{air}}\right]_{\overline{E}_{(X-ray)}}}{\left[\frac{(\mu_{en}/\rho)_{LiF}}{(\mu_{en}/\rho)_{PMMA}}\right]_{ref}} \quad (4)$$

where $N_K \ (\mu\text{Sv.nC}^{-1})\big|_{\overline{E}_{(X-ray)}}$ is the calibration factor of the dosimeter at X-ray field with mean energy of $\overline{E}$, N_K $(\mu\text{Sv.nC}^{-1})\big|_{ref}$ is the calibration factor of the dosimeter calibrated in a Co-60 reference field with $\overline{E}$ of 1.25 MeV. $(\mu_{en}/\rho)_{air}$, $(\mu_{en}/\rho)_{PMMA}$, and $(\mu_{en}/\rho)_{LiF}$ are related to mass energy absorption coefficients of the air, PMMA

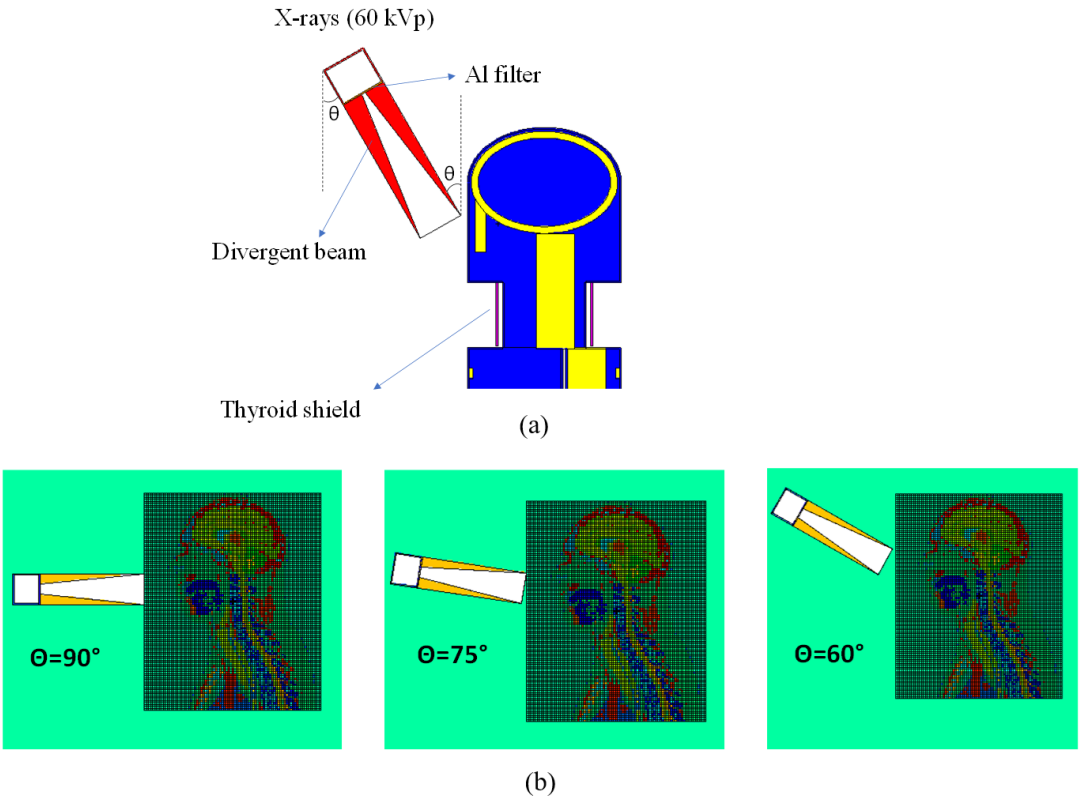

Figure 3: Illustration of the actual simulation geometry implemented in the MCNP code for periapical radiography using a 60 kV X-ray tube, (a) at vertical angle of θ relative to the face, utilizing the MIRD phantom to estimate the absorbed dose in the thyroid gland at the presence of the thyroid shield with 4 mm thickness, and divergent beam with length of 20 cm (red, blue, and yellow materials in the phantom are related to thyroid shield made of composite or lead, soft tissue, and bone, respectively), and (b) at various angles of $\theta = 60°$, 75°, and 90°.

(phantom media), and LiF dosimeter (TLDs -GR200) at specified energies, in which were obtained by interpolation of the NIST standard tables (Hafezi et al., 2018; Berger et al., 2010).

2.4 Simulation methodology

The experimental setup employed a fixed vertical angulation of 60°, which represents a typical configuration for maxillary molar periapical radiography. However, clinical periapical imaging involves a range of tube angulations, which may influence the degree of scatter reaching the thyroid and thus the relative shielding effectiveness. So, various angles (including 60°, 75°, and 90°) were simulated using the Monte Carlo simulations by MCNP code with a Korean adult male phantom, adapted from the anthropomorphic ORNL MIRD model, for dose calculations (Park et al., 2006; Han et al., 2006). The thyroid gland cell was defined with a 19.9 cm^3 volume and 1.05 $g.cm^{-3}$ density, using a material composition including hydrogen (10.4%), carbon (11.9%), nitrogen (2.4%), oxygen (74.5%), and trace elements comprising Na (Sodium), P (Phosphorus), S (Sulfur), Cl (Chloride), K (Potassium), and I (Iodine). Also, the composite, made of 70 wt% Bi_2O_3/SR, includes 2.4% Hydrogen (H), 9.7% Carbon (C), 13.7% Oxygen (O), 11.4% Silicon (Si), and 62.8% Bismuth (Bi). Also, the 70wt% Bi_2O_3/SR composite was defined in the MCNP code including weight fractions of H: 0.02447, C: 0.09718, O: 0.13683, Si: 0.11363, and Bi: 0.62789. In the simulation section, to enable a fair comparison between the composite shield developed in this study and commercial thyroid shields (equivalent to 0.5 mm Pb), pure lead with a thickness of 0.5 mm was employed as the reference material for commercial shield. This approach was adopted due to the lack of access to the exact proprietary composition and formulation of commercially available thyroid collars. In Fig. 3, depiction of the simulation setup and irradiation method in periapical radiography at various angles is presented, where $\theta = 90°$ is related to the case that the X-ray tube is located at horizontal plane parallel to the floor. The X-ray source was modeled as a point source (focal spot 0.5×0.5 mm^2) emitting a divergent beam (incomplete cone, length 20 cm, output diameter 6 cm) with an aluminum filter (2.66 mm thick). Simulations used monoenergetic photons at 60 keV (maximum energy) with appropriate physics cards (mode p e) to account for the spectrum effects.

Although the simulations were based on monoenergetic photons corresponding to the maximum photon energy of 60 keV, an aluminum filter with a thickness of 2.66 mm (density 2.70 $g.cm^{-3}$) was also taken into account due to its effect on the energy spectrum. Additionally, a divergent beam, configured as an incomplete cone geometry with a length of 20 cm, was defined at the output of the tube such that its output diameter is 6 cm (with an input

Table 3: Results of simulation to assess the absorbed dose in thyroid gland in periapical (Intra-oral) radiology at 60 kV, 7 mA, 0.32 s, at various angles.

Thyroid shield type	Absorbed dose in thyroid gland (μGy)					
	Angle 60°	Dose reduction (%)	Angle 75°	Dose reduction (%)	Angle 90°	Dose reduction (%)
Unshielded	1708.3±23.6	-	128.1±1.8	-	119.6±1.7	-
Commercial shield (Equivalent to 0.5 mm Pb)	253.9±3.5	85.1	108.6±1.5	15.2	99.7±1.4	16.6
Composite shield (This work)	285.2±3.9	83.3	109.3±1.5	14.7	100.2±1.4	16.2

diameter of 2 cm).

To evaluate the radiation shielding effectiveness of the composites shield for protection of thyroid gland, a polymer/heavy metal oxide composite with thickness of 4 mm (density 2.68 g.cm^{-3}) composed 70 wt% Bi_2O_3 in silicone rubber was introduced by cylindrical surfaces encompassing the thyroid region. X-rays were exposed towards the phantom's jaw from the front at various angles with respect to the face. Photon and electron transport were simulated in mode p e, incorporating physics cards for coherent scattering and electron interactions. In the MCNP simulations, the absorbed dose to the thyroid gland was scored using the F6:p tally (energy deposition in MeV/g per source photon). The FM6 multiplier card was applied to convert the results to absolute dose in Gy, incorporating both the unit conversion (MeV.g^{-1} to Gy) and the tube current of 7 mA used in the experimental setup. This scaling ensures consistency with the irradiation conditions (60 kV, 7 mA, 0.32 s exposure time). This setup accounted for scatter from surrounding tissues, modeled with densities of 1.04 g.cm^{-3} (soft tissue), 1.40 g.cm^{-3} (bone), and 0.296 g.cm^{-3} (lungs).

3 Results and discussion

3.1 Simulation results

In Table 3, results of Monte Carlo simulation to assess the absorbed dose in the thyroid gland in periapical (Intra-oral) radiology at 60 kV, 7 mA, 0.32 s, at various vertical angles are exhibited. The Monte Carlo simulations were conducted both with and without a thyroid shield at three representative angles using the MCNP code. The effect of irradiation angle on thyroid absorbed dose can be interpreted as follows: Sub-optimal angulation significantly influences the thyroids exposure to the primary beam, often more than the presence of a shield itself (Worrall et al., 2018).

In the present work, at the experimental phase, the angle for diagnostic image quality in periapical radiography was determined to be 60°, as this angulation provides the best combination of root coverage, minimal foreshortening/elongation, and acceptable superimposition of anatomical structures. In the simulation phase, as can be seen from Table 3, at angle of 60°, the unshielded thyroid absorbed dose reached 1708.3±23.6 μGy because a considerable portion of the gland lies within or close to the primary beam path.

Deviations toward higher angles (near to horizontal line or floor) markedly reduce thyroid exposure. At 75°, the unshielded thyroid dose decreases by approximately 92.5% to 128.1±1.8 μGy, and at 90° (horizontal situation) it falls further to 119.6±1.7 μGy (a 93% reduction relative to 60°). These substantial reductions occur because progressively less of the thyroid is intersected by the primary beam, shifting the majority of the exposure to the oral mucosa, alveolar bone, and salivary glands.

The application of thyroid shielding proves highly effective precisely at the optimal 60° angle: both the commercial shield (0.5 mm Pb equivalent) and the composite shield developed in this study reduce thyroid dose by 83-85% (to 253.9285.2 μGy). In contrast, at 75° and 90° angles -where the thyroid dose is already inherently low- shielding yields only modest additional benefit (14.716.6% further reduction), with no clinically meaningful difference between the two shield types.

While steeper angulations (75°, and 90°) dramatically lower thyroid dose, they compromise diagnostic image quality through increased distortion, overlap of zygomatic processes, and potential loss of apical detail, which may necessitate repeat exposures and ultimately negate the dosimetric advantage. The study therefore emphasizes that precise adherence to the optimal 60° angulation -combined with routine use of thyroid shielding- represents the most effective strategy to achieve diagnostic image quality while simultaneously minimizing absorbed dose to the thyroid and adjacent radiosensitive structures (salivary glands, esophagus, and bone marrow). Accurate beam angulation at the established optimum must remain the primary dose-reduction measure in Intra-oral periapical radiography, supplemented by appropriate shielding whenever feasible. The simplified nature of the simulation has been recognized. It is emphasized that, although the simulation and experimental results do not match exactly in terms of the absorbed dose values in the thyroid gland, the primary value of the simulation lies in its ability to predict trends in relative dose reduction across different angulations. It is acknowledged that absolute dose values differ due to variations in phantom models (MIRD versus Rando) and beam modeling (monoenergetic versus polyenergetic). The simulations were primarily employed to evaluate relative shielding efficacy across different angulations, which aligns well with the observed experimental trends.

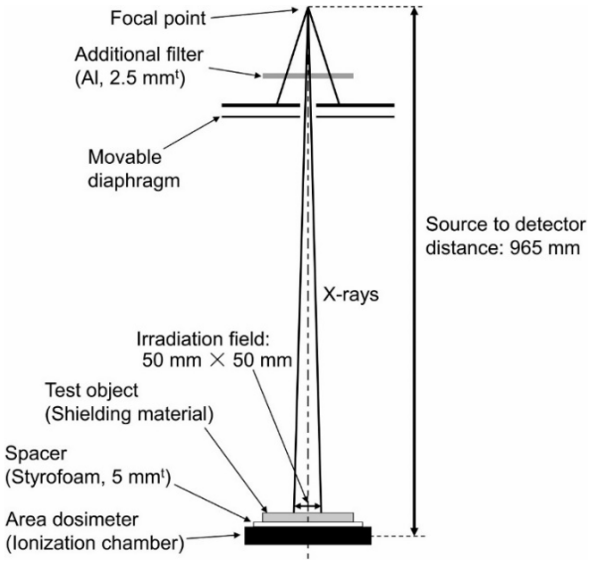

Figure 4: Illustration of the experimental setup based on the inverse broad-beam condition (IEC 61331-1, 2014; IEC 61331-3, 2014).

3.2 Experimental results

3.2.1 Evaluation of X-ray shielding ability using the inverse broad-beam geometry

The IEC 61331-1 standard defines three distinct geometric conditions for measuring the attenuation ratio of protective materials against diagnostic X-rays (IEC 61331-1, 2014). The narrow beam condition is designed to isolate and measure attenuation due solely to primary photons. By using specific diaphragms and a sufficient detector distance, it minimizes the probability that secondary photons -such as those from Compton scattering or fluorescence emitted by the test material- reach the radiation detector. In contrast, the broad-beam condition maximizes the detection of these secondary photons (Compton and fluorescence), reflecting a more realistic scenario where scattered radiation contributes to the total exposure behind the shielding. The inverse broad-beam condition employs a narrow beam incident on a small material sample coupled with a large-area flat detector immediately behind it. This method, suitable for voltages up to 150 kV and often used for protective clothing, effectively captures both primary and secondary radiation components while offering practical advantages like lower measurement uncertainty and the need for only small material samples. Each condition thus provides a different perspective on material performance by selectively including or excluding the influence of scattered and fluorescent radiation (IEC 61331-1, 2014). In this research, the inverse broad-beam geometry was selected to conduct tests on thyroid collars, including the composite shield. The inverse broad-beam measurements, as a globally recognized standard test method, have widespread application in assessing the shielding performance of protective devices against diagnostic medical X-rays (Maeda et al., 2022).

Figues 4 and 5 illustrate the experimental setup employing inverse broad-beam geometry based on the IEC 61331 at the SSDL of Iran (IEC 61331-1, 2014; IEC 61331-3, 2014). The evaluation of X-ray shielding performance was conducted using diagnostic X-ray equipment (COMET MXR 320/26 irradiation system). The source-to-dosimeter distance was set at 965 mm. A lead diaphragm with a circular aperture of 65 mm diameter and 6.5 mm thickness, incorporated within a plate measuring 15 × 15 cm^2, was positioned at a distance of 475 mm from the focal spot. The X-ray beam corresponded to the RQR5 radiation quality as defined by IEC 61267, utilizing a tube voltage of 70 kV, mean photon energy 39.4 keV (Ankerhold et al., 2009), additional filtration equivalent to 2.5 mm aluminum (measured at a distance of 400 mm from the focal spot), and exhibiting a half-value layer (HVL) of 2.58 mm aluminum (IEC, 2005). Additional experimental parameters included a tube current of 5 mA, an exposure duration of 30 s, and an irradiation field size of 50 mm × 50 mm. To measure the air kerma rate, a 0.6 cc PTW Farmer-type ionization chamber was employed. The collected electric charge was measured over 30-second intervals using a PTW-Unidose E electrometer operated at a bias voltage of +400 V. Additionally, the ambient temperature and pressure during irradiation were recorded as 16.8 °C and 849 mbar, respectively.

Table 4 presents measurements of air kerma rate based on the reference radiation quality of RQR5 (70 kV, 5 mA, 30 s) at the SSDL of Iran, evaluating the efficacy of various thyroid shields in reducing scattered radiation exposure. The unshielded scenario yielded an air kerma rate of 20.596±0.95 $mGy.min^{-1}$, serving as the baseline. The composite thyroid shield developed in this study demonstrated exceptional performance, reducing the air kerma rate to 0.0071±0.0003 $mGy.min^{-1}$, achieving a 99.97% dose reduction. In comparison, a commercial shield equivalent to 0.5 mm lead attenuated the rate to 0.1898±0.0087 mGy/min, resulting in a 99.08% reduction. Finally, pure lead shielding of 0.5 mm thickness provided a rate of 0.3843±0.0177 mGy/min, corresponding to a 98.13% reduction. These results indicate that the composite shield offers superior radiation protection compared to both the commercial equivalent and pure lead, with substantially lower transmitted doses and higher percentage reductions, highlighting its potential for enhanced safety in clinical settings involving ionizing radiation.

The superior performance observed under standard broad-beam conditions supports the claim of enhanced shielding efficacy and is likely attributable to reduced backscattered radiation in bismuth. Furthermore, the phantom-based experiments, conducted using the Rando phantom, reflect clinically realistic broad-beam scatter conditions in periapical radiography, whereas the SSDL data provided are based on standardized broad-beam validation.

3.2.2 Measurement at Preapical, and OPG centers

Results of irradiation and measurement for the composite shield were compared with those of a commercial thyroid collar, which is equivalent to 0.5 mm Pb. Addition-

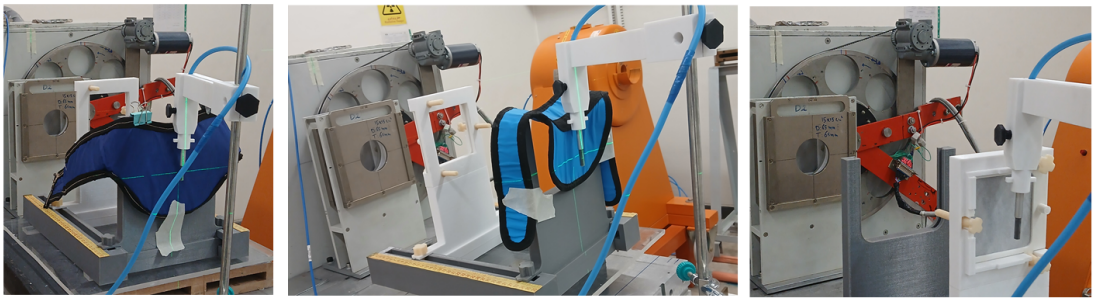

(a) (b) (c)

Figure 5: Experimental setup at the SSDL of Iran, in accordance with the IEC 61331, for evaluation of X-ray shielding ability of various shields including: a) Composite shield (this work), b) Commercial shield (equivalent to 0.5 mm Pb), and c) Lead sheet (with thickness of 0.5 mm).

Table 4: Measurement of air kerma rate recommended by the IEC 61331 based on the reference radiation quality of RQR5 (70 kV, 5 mA, 30 s) at the SSDL of Iran using various shields.

Type of thyroid shield	Air kerma rate ($mGy.min^{-1}$)	Dose reduction (%)
Unshielded	20.596±0.95	-
Composite shield (This work)	0.0071±0.0003	99.97
Commercial shield (equivalent to 0.5 mm Pb)	0.1898±0.0087	99.08
Pure lead (0.5 mm Pb)	0.3843±0.0177	98.13

ally, the Rando phantom was irradiated without a thyroid shield to thoroughly assess the shielding effectiveness of both the composite and commercial shields. Figure 6 illustrates the initial intensity readings obtained from the TLD GR-200 dosimeters across various channels for the thyroid gland within a periapical device operating at 60 kV, 7 mA, and 0.32 s using the Rando phantom for three positions namely, without shield, composite shield, and a conventional lead shield. As can be seen from Fig. 6, the area under the intensity curve, as a function of the channel number is greatest for the unshielded condition around channel # 210-230. This indicates that the thyroid gland receives the maximum dose for unshielded position in comparison with other conditions, qualitative. Following this, the conventional lead shield and then the composite thyroid shield are ranked in order. The lowest area under the curve corresponds to the composite thyroid shield (in this study), indicating that the thyroid gland receives the minimum dose when this shield is utilized.

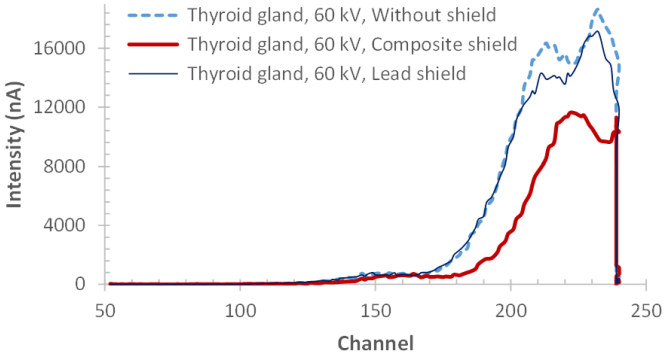

Figure 6: Comparison of TLD-GR200 reading in thyroid gland, without shield, composite shield, and a conventional lead shield in a periapical device.

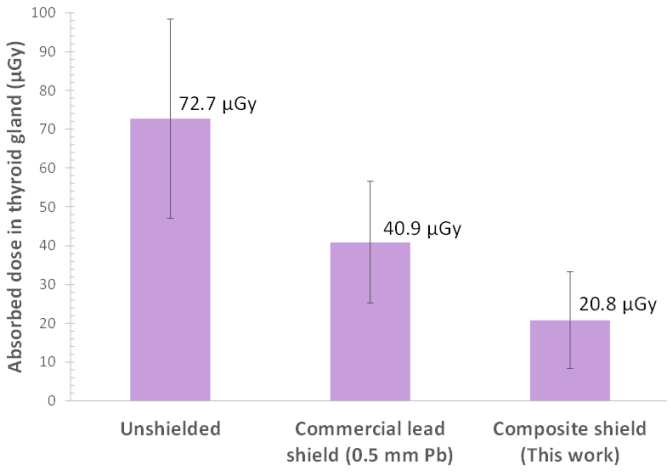

Figure 7: Total dose in thyroid gland in periapical device, for unshielded, commercial shield, and the composite shield in this work.

Table 5 illustrates the experimental findings of dose measurements in the superior, inferior, and total thyroid gland, both with and without protective collars, utilizing a conventional periapical device in conjunction with the Rando phantom, where the composite shield is positioned at the front of the phantom's neck (Fig. 2). The study evaluates three conditions: Unshielded: No thyroid shield was used, serving as the baseline for comparison. Commercial shield (0.5 mm Pb): A standard lead-based thyroid shield with a thickness of 0.5 mm. Composite shield: A shield made of 70 wt% Bi_2O_3/silicone rubber composite, potentially offering different radiation attenuation properties compared to lead. Dose measurements were conducted at two specific locations in the thyroid gland: superior (Slice #9), and inferior (Slice #10) re-

Table 5: Results of experimental measurements using TLD-GR200 dosimeters in periapical radiology at 60 kV, 7 mA, 0.32 s, and comparison with other studies.

Conditions of exposure	Thyroid shield type	Measured dose in thyroid (μGy)			Dose reduction (%)	Ref.
		Superior (Slice#9)	Inferior (Slice#10)	Total Total		
60 kV, 7 mA, 0.32 s	Unshielded	68.5±17	76.9±15.6	72.7±25.7	-	This work (Experiment)
60 kV, 7 mA, 0.32 s	Commercial shield (0.5 mm Pb)	66.1±15.6	15.8±3.2	40.9±15.6	43.7	This work (Experiment)
60 kV, 7 mA, 0.32 s	Composite shield	33±1.8	8.6±3.0	20.8±12.5	71.4	This work (Experiment)
70 kV, 7 mA, 0.1 s	Unshielded	-	-	23.2	-	(Hoogeveen et al., 2016)
70 kV, 7 mA, 0.1 s	Commercial lead shield (round collimation for upper canine at angle of 45)	-	-	6.9	70.2	(Hoogeveen et al., 2016)
60 kV, 7 mA, 0.5 s	Unshielded	-	-	18.2	-	(Worrall et al., 2018)
60 kV, 7 mA, 0.5 s	Bismuth shield	-	-	13.7	24.7	(Worrall et al., 2018)

lated to the upper and lower parts of the thyroid gland, respectively. The total dose in thyroid gland was measured by averaging the dose in superior, and inferior parts.

As can be seen from Table 5, and Fig. 7, the amounts of dose in thyroid gland for various positions including unshielded, a commercial lead shield, and composite shield are 72.7±25.7 μGy (35.3% expanded uncertainty, coverage factor of $k = 1$), 40.9±15.6 μGy (74.5% expanded uncertainty, coverage factor of $k = 1$), and 20.8±12.5 μGy (59.9% expanded uncertainty, coverage factor of $k = 1$), respectively.

The implementation of composite shielding resulted in a 71.4% dose reduction, compared to 43.7% for the commercial collar. Although the shielding effectiveness of the composite thyroid collar against the 60 kV dental X-rays is significantly higher than that of the commercial equivalent with 0.5 mm Pb, it should be noted that-based on the Table 1- the weight of the composite shield (600 grams) is greater than that of the commercial shield ($\sim$ 400 g). It is recommended that future research focus more on optimizing the thickness during the manufacturing process to ensure uniform distribution of bismuth oxide filler particles within the silicone rubber matrix while maintaining sufficient flexibility. This approach could enable the production of a thyroid shield with a lighter weight compared to commercial lead-containing shields.

The composite shield reduced the superior thyroid dose by 50% compared to the lead shield, demonstrating better attenuation. To justify the considerable uncertainty in the measurement of absorbed dose within the thyroid gland, there was a notable difference in the dose between the superior and interior parts of the thyroid. Ultimately, the average absorbed dose in these areas was reported as the total dose for the thyroid gland. The high standard deviation in the total dose (74.5%) indicates variability, possibly due to shield positioning or anatomical differences.

Findings of Hoogeveen et al. (Hoogeveen et al., 2016), and also Aytugar et al. (Aytugar et al., 2018), revealed a reduction in thyroid dose in periapical cases as 70.2%, and 63.9%, respectively, aligning with this studys findings. Comparative studies used slightly different settings (70 kV, 7 mA, with exposure times of 0.1 s or 0.2 s), which may influence dose measurements due to variations in radiation intensity and duration. For example, Hoogeveen et al. (Hoogeveen et al., 2016), obtained the unshielded dose in thyroid as 23.2 μGy, in which is significantly lower than in this study 72.7 μGy, likely due to the shorter exposure time (0.1 s vs. 0.32 s). It is worth noting that in order to convert dose equivalent (Sv) to absorbed dose (Gy), it is sufficient to divide the equivalent dose by conversion factors from air kerma to operational dose equivalent quantities for low-energy X-rays (IAEA, 2018; Hakanen et al., 2007).

It should be noted that the increased dose by the superior part of the thyroid gland when using composite and conventional lead shields can be attributed to its proximity to the X-ray focal point. This phenomenon was noted in the research conducted by Hafezi et al., who examined the radiation exposure in the thyroid gland while utilizing various protective collars during dental radiography (Hafezi et al., 2018).

In periapical (Intra-oral) radiography, the relative importance of thyroid shielding is indeed lower than in panoramic imaging (OPG), primarily due to the irradiation geometry. Regardless of whether a shield is present, a considerable fraction of the X-ray beam -both directly

and via internal scatter within the head and neck- reaches the thyroid gland because of the steeper cranial angulation and the proximity of the primary beam exit path to the thyroid region.

3.2.3 Mechanism of dose reduction in bismuth composite in comparison with lead

The primary objective of the thyroid shield is to attenuate radiation exposure to the thyroid gland during periapical radiography, where the gland receives dose predominantly from scattered X-rays rather than the direct primary beam. In periapical imaging, the X-ray tube is positioned to direct the primary beam toward the intraoral region (e.g., teeth and jaw) at a typical vertical angulation of 60° relative to the face. The primary beam interacts with tissues in the head and neck, generating scattered radiation through Compton scattering, where photons deviate from their original path upon collision with electrons in the patient's tissues. This scattered radiation, originating mainly from the oral mucosa, alveolar bone, and salivary glands, propagates isotropically and reaches the thyroid gland located inferiorly in the neck.

As can be seen from Fig. 8, it is possible that the polymer-based composite shield containing bismuth oxide developed in the present study offers an additional advantage over conventional lead-equivalent shields: a relative lower yield of backscattered radiation from bismuth may be results in decreased secondary exposure of the thyroid gland from photons scattered backward from the shield itself. This mechanism likely contributes to the observed further reduction in thyroid absorbed dose compared to the lead-based commercial shields. Also, bismuth has an atomic number ($Z = 83$) slightly higher than lead ($Z = 82$), resulting in a marginally greater photoelectric absorption cross-section for diagnostic X-rays (energies ~30-150 keV) (Malekie et al., 2022). The photoelectric process is the predominant mode of interaction for X-rays of relatively low energy. The photoelectric effect, where photons are fully absorbed by inner-shell electrons, scales approximately with $Z^n/E^{3.5}$, in which the exponent n varies between 4 and 5 over the energy region of E (Knoll, 2010). This leads to more efficient energy deposition in bismuth without producing significant scattered photons. In broad-beam conditions, this manifests as lower absorbed doses, as observed in the SSDL measurements (99.97% reduction for Bi_2O_3 composite vs. 99.08% for lead-equivalent).

Furthermore, the dose reduction factor exhibits an inverse relationship with the particle size of the filler material (Maeda et al., 2022), namely bismuth oxide. This means that as the particle size of the filler decreases, the dose reduction factor increases. Given that the particle size of Bi_2O_3 in the composite shield is approximately 5 μm (Shahbazi et al., 2026), it is possible that the composite shield demonstrates a greater dose reduction compared to the lead shield.

Figure 8: Schematic illustration of the mechanism by which bismuth shielding reduces the absorbed dose to the thyroid gland during periaperal radiography, primarily due to its substantially lower backscattered radiation compared with lead.

It should be mentioned that the exposure of thyroid gland during periapical dental imaging may arise from various sources, including primary radiation beams, as well as internal and external scattered radiation. The degree of radiation exposure is significantly modulated by several pivotal factors, including the specific model of the periapical imaging device, the angular exposure in radiation delivery, and the properties of the shielding materials utilized, encompassing their composition and structural design (Hafezi et al., 2018). These factors collectively contribute to reducing the risks associated with thyroid radiation exposure. To enhance patient safety, meticulous attention should be directed toward the selection of imaging equipment, precise adjustment of exposure angles, and the implementation of shielding materials specifically engineered to minimize unwarranted radiation exposure while preserving diagnostic accuracy. Results of the previous research by the authors for the OPG device revealed that the thyroid gland received an absorbed dose of 386.6±219.8 μSv without shielding, 19.0±12.4 μSv with the composite shield, and 37.9±18.7 μSv with a commercial thyroid collar (equivalent to 0.5 mm Pb), respectively (Shahbazi et al., 2026). This represented a 95.1% dose reduction when the composite shield was used, which proved 5.4% more effective than the commercial thyroid collar (Shahbazi et al., 2026). Results of this study indicates that the composite shield, which achieves a 95.1% reduction in dose for OPG, demonstrates superior efficacy compared to periapical radiography, with 71.4% dose reduction in the thyroid gland.

3.3 Estimation of uncertainty

In the experimental phase, four TLD dosimeters were placed on each of the two thyroid-containing slices (slice #9 and slice #10), resulting in a total of eight TLDs dedi-

cated to the thyroid gland. Measurements in slice #9 provided the absorbed dose in the superior part of the thyroid, while measurements in slice #10 provided the absorbed dose in the inferior part. On each slice, the four TLDs were positioned at the center, right, left, and anterior aspects of the thyroid region. In each slice, the average reading of the four placed dosimeters was recorded. Since only one irradiation was performed for each shielding configuration (unshielded, commercial shield, composite shield), the uncertainty associated with the dose measurement for each individual slice was derived solely from the four TLD readings obtained on that slice during this single exposure. The standard uncertainty for the mean dose of one slice was calculated as the standard deviation of these four TLD readings exhibiting the Type A uncertainty, reflecting random spatial variations of dose within the thyroid tissue of a single slice under the same irradiation conditions. The expanded uncertainty arising from the average of the four samples (reported as error) is presented in Table 5.

In addition to Type A uncertainty, there are several Type B uncertainties including TLD calibration coefficient at the SSDL ($< 3\%$), linearity response ($< 1\%$), reader repeatability and stability ($< 1\%$), energy-response correction ($< 5\%$), inhomogeneity of dosimeter sensitivity or ECC ($< 5\%$), fading correction ($< 5\%$ per year), natural background radiation ($< 2\%$), and spatial variation or positioning namely 4 TLDs/slice (34%, 73.9%, and 59.1% for unshielded, commercial lead shield, and composite shield, respectively). It should be noted that, as described in Section 2.2, the TLD dosimeters were placed on the surfaces of phantom slices #9 and #10. This placement may have increased the uncertainty in estimating the absorbed dose to the thyroid gland, as accurate positioning within the designated locations was not feasible.

In addition to the aforementioned factors contributing to measurement uncertainty, it is pertinent to note that in the present study, the calibration of TLD-GR200 dosimeters was performed operationally in the presence of gamma-rays from a Co-60 source at the SSDL in Iran. However, the calibration coefficient was determined for radiographic X-ray beams through computational conversions. The contribution of scatter (or backscattered) radiation in X-ray fields is greater due to the lower energy compared to gamma-rays (1250 keV). This significant factor effectively increases the uncertainty, although in most published articles, the energy dependence-related uncertainty for TLD-GR200 dosimeters has been reported to be less than 5% (Alizadeh et al., 2022; Sadeghi et al., 2025; Navab et al., 2016). Notably, the dosimetric characteristics of the TLD-GR200 dosimeters including energy, angular, and linearity dependency, and also associated sources of uncertainty have been extensively reviewed in the literature (Alizadeh et al., 2022; Sadeghi et al., 2025; Navab et al., 2016).

The combined uncertainty for the final thyroid dose (average of the eight TLD readings from both slices) was obtained by quadratically combining the Type A uncertainty (derived from the spatial variation among the four TLDs per slice) with all relevant Type B components through Eq. (5) (Sadeghi et al., 2025):

$$U_c = \sqrt{(U_A)^2 + (U_B)^2} \tag{5}$$

In which, U_A, and U_B are related to Type A, and Type B components of the uncertainty. This combined uncertainty then should be multiplied by a coverage factor (k) to provide an expanded uncertainty (U) (Sadeghi et al., 2025):

$$U = k.U_c \tag{6}$$

Typically, expanded uncertainty is reported at a coverage factor of $k = 2$, corresponding to an approximate 95% level of confidence. In the present work, however, a coverage factor of $k = 1$ has been applied due to significant spatial variation and positioning effects, resulting in a 68% level of confidence, in accordance with the Guide to the Expression of Uncertainty in Measurement (GUM) (Pooya and Orouji, 2014; ISO/IEC Guide 98-3:2008, 2008).

4 Conclusions

In summary, this study demonstrates that a lead-free thyroid shield based on 70 wt% micro-sized Bi_2O_3 dispersed in silicone rubber significantly outperforms conventional 0.5 mm Pb-equivalent commercial collars in periapical dental radiography. At the clinically relevant 60° vertical angulation, the composite shield reduced the thyroid absorbed dose by 71.4%, compared to 43.7% for the commercial collar. Monte Carlo simulations using the MCNP code with a modified MIRD phantom confirmed high attenuation, showing dose reductions of 83.3% with the composite shield and 85.1% with the commercial (equivalent to 0.5 mm Pb) shield at 60° angulation. Simulations at higher angles (75° and 90°) revealed inherently lower unshielded doses due to reduced primary beam intersection with the thyroid, with shielding providing only modest additional benefit, underscoring the importance of optimal angulation combined with shielding for maximal protection. Additionally, under standardized SSDL inverse broad-beam conditions based on IEC 61331 (RQR5 radiation quality, 70 kV), the composite shield demonstrated exceptional performance, reducing the air kerma rate by 99.97%, compared to 99.08% for the commercial shield and 98.13% for 0.5 mm pure lead. This superior attenuation is likely attributable to reduced backscattered radiation from bismuth relative to lead.

The superior performance of the Bi_2O_3/silicone rubber composite, demonstrated across phantom experiments, Monte Carlo simulations, and standardized broad-beam testing, confirms its enhanced shielding efficacy while eliminating lead-related toxicity and environmental hazards. Although its weight is comparable to conventional lead shields and may impair comfort -particularly in pediatric, geriatric, or anxious patients- it restricts neck movement, serving as a stabilizing device to prevent motion during brief radiographic exposures (seconds). Key limitations include weight and ergonomic challenges. Future research should prioritize weight reduction via optimized filler loading, improved particle dispersion for uniform thinner shields, or layered designs that preserve attenuation efficiency.

Acknowledgements

The authors express their gratitude to the staff of Nuclear Science and Technology Research Institute (NSTRI) for TLD services, and also Sepid Partov Radiology Center, particularly to Dr. P. Rezaeian, Dr. A. Moslehi, Ms. Vahabi, and Dr. S. Goorang.

Conflict of Interest

The authors declare no potential conflict of interest regarding the publication of this work.

Funding

The authors declare that no funds, grants, or other financial support were received during the preparation of this manuscript.

References

(2024). Thyroid collar standard. https://www.meddeal.in/91701-thyroid-collar-standard.html.

Aghaz, A., Faghihi, R., Mortazavi, S., et al. (2016). Radiation attenuation properties of shields containing micro and Nano WO3 in diagnostic X-ray energy range. *International Journal of Radiation Research*, 14:127.

Aghaz, A., Kardan, M., Deevband, M., et al. (2018). Comparison of two different methods for CTDIw calculation in CBCT systems. *Iranian Journal of Medical Physics*, 15:224–224.

Aghaz, A., Kardan, M., Deevband, M., et al. (2021). Patient-specific dose assessment using CBCT images and Monte Carlo calculations. *Journal of Instrumentation*, 16:P10011.

Al-Buriahi, M., Kavaz, E., Perianolu, U., et al. (2021). SrO effect on photon/particle radiation protection characteristics of SrO-PbO-B2O3 glasses. *Journal of Inorganic and Organometallic Polymers and Materials*, 31:4546–4562.

Alizadeh, M., Mohseni, M., Farhood, B., et al. (2022). Thermoluminescent characteristics of GR-200, TLD-700H and TLD-100 for low dose measurement: linearity, repeatability, dose rate and photon energy dependence. *Journal of Biomedical Physics & Engineering*, 12:111.

Ankerhold, U., Hupe, O., and Ambrosi, P. (2009). Deficiencies of active electronic radiation protection dosemeters in pulsed fields. *Radiation Protection Dosimetry*, 135:149–153.

Attix, F. (2008). *Introduction to radiological physics and radiation dosimetry*. John Wiley & Sons.

Aytugar, E., Kose, T., Gumru, B., et al. (2018). Are bismuth shields useful in dentomaxillofacial radiology practice for the protection of eyes and thyroid glands from ionizing radiation? *Iranian Journal of Radiology*, 15.

Bawazeer, O., Almutairi, H., Almutiri, K., et al. (2024). Radiation protection in dental imaging: Evaluating the impact of the SABA thyroid shield during panoramic and cone beam computed tomography. *Journal of Radiation Research and Applied Sciences*, 17:101102.

Berger, M. and Hubbell, J. (1987). XCOM: Photon cross sections on a personal computer. Technical report, National Bureau of Standards, Washington, DC (USA). Center for Radiation.

Berger, M., Hubbell, J., Seltzer, S., et al. (2010). XCOM: Photon Cross Section Database. Technical report, National Institute of Standards and Technology, Gaithersburg, MD.

Charles, M. (2010). *Effects of Ionizing Radiation: United Nations Scientific Committee on the Effects of Atomic Radiation: UNSCEAR 2006 Report, Volume 1Report to the General Assembly, with Scientific Annexes A and B*. Oxford University Press.

Demir, L., Perianolu, U., and ahin, M. (2019). Investigating XRF parameters and valance electronic structure of the Co, Ni, and Cu spinel ferrites. *Ceramics International*, 45:7748–7753.

Demirel, . and Ycel, H. (2024). Development of a flexible composite based on vulcanized silicon casting with bismuth oxide and characterization of its radiation shielding effectiveness in diagnostic X-ray energy range and medium gamma-ray energies. *Nuclear Engineering and Technology*, 56:2570–2575.

Eder, H. and Schlattl, H. (2018). IEC 61331-1: A new setup for testing lead free X-ray protective clothing. *Physica Medica*, 45:6–11.

Einstein, A., Elliston, C., Groves, D., et al. (2012). Effect of bismuth breast shielding on radiation dose and image quality in coronary CT angiography. *Journal of Nuclear Cardiology*, 19:100–108.

Gholamzadeh, L., Asari-Shik, N., Aminian, M., et al. (2020). A study of the shielding performance of fibers coated with high-Z oxides against ionizing radiations. *Nuclear Instruments and Methods in Physics Research Section A: Accelerators, Spectrometers, Detectors and Associated Equipment*, 973:164174.

Hafezi, L., Arianezhad, S., and Pooya, S. H. (2018). Evaluation of the radiation dose in the thyroid gland using different protective collars in panoramic imaging. *Dentomaxillofacial Radiology*, 47:20170428.

Hakanen, A., Kosunen, A., Pyry, P., et al. (2007). Determination of conversion factors from air kerma to operational dose equivalent quantities for low-energy X-ray spectra. *Radiation Protection Dosimetry*, 125:198–204.

Han, E., Bolch, W., and Eckerman, K. (2006). Revisions to the ORNL series of adult and pediatric computational phantoms for use with the MIRD schema. *Health Physics*, 90:337–356.

Hoogeveen, R., Hazenoot, B., Sanderink, G., et al. (2016). The value of thyroid shielding in intraoral radiography. *Dentomaxillofacial Radiology*, 45:20150407.

Hosseini, M., Malekie, S., and Kazemi, F. (2022). Experimental evaluation of gamma radiation shielding characteristics of Polyvinyl Alcohol/Tungsten oxide composite: A comparison study of micro and nano sizes of the fillers. *Nuclear Instruments and Methods in Physics Research Section A: Accelerators, Spectrometers, Detectors and Associated Equipment*, 1026:166214.

IAEA (2018). *Occupational Radiation Protection, IAEA Safety Standards Series No. GSG-7*. IAEA, Vienna.

IEC (2005). IEC 61267, Medical diagnostic X-ray equipment - Radiation conditions for use in the determination of characteristic. Technical report, International Electrotechnical Commission.

IEC 61331-1 (2014). Protective devices against diagnostic medical X-radiation - Part 1: Determination of attenuation properties of materials. Technical report, International Electrotechnical Commission.

IEC 61331-3 (2014). Protective devices against diagnostic medical X-radiation - Part 3: Protective clothing, eyewear and protective patient shields. Technical report, International Electrotechnical Commission.

ISO/IEC Guide 98-3:2008 (2008). *Uncertainty of measurement - Part 3: Guide to the expression of uncertainty in measurement (GUM:1995)*. ISO and IEC.

Janani, K., Malarkodi, T., and Sankarapandian, S. (2021). Estimation of Surface Radiation Dosage to Thyroid Gland and Lower Abdomen While Using Intraoral Periapical Radiography: A Phantom Study. *Cureus*, 13.

Jayakumar, S., Saravanan, T., and Philip, J. (2023). A review on polymer nanocomposites as lead-free materials for diagnostic X-ray shielding: Recent advances, challenges and future perspectives. *Hybrid Advances*, page 100100.

Kelaranta, A., Ekholm, M., Toroi, P., et al. (2016). Radiation exposure to foetus and breasts from dental X-ray examinations: effect of lead shields. *Dentomaxillofacial Radiology*, 45:20150095.

Kim, S., Frush, D., Yoshizumi, T., et al. (2010). *Pediatric Radiology*, 40:1739–1743.

Knoll, G. (2010). *Radiation Detection and Measurement*. John Wiley & Sons, Inc, 4th edition.

Lee, Y., t. Park, E., Cho, P., et al. (2011). Comparative analysis of radiation dose and image quality between thyroid shielding and unshielding during CT examination of the neck. *American Journal of Roentgenology*, 196:611–615.

Ludlow, J., Davies-Ludlow, L., and White, S. (2008). Patient risk related to common dental radiographic examinations: the impact of 2007 International Commission on Radiological Protection recommendations regarding dose calculation. *The journal of the American Dental association*, 139:1237–1243.

Maeda, T., Hayashi, H., Lee, C., et al. (2022). Experimental study of X-ray dose reduction factor when using various size bismuth and lead particles. *Radiation Physics and Chemistry*, 195:110049.

Malekie, S., Shooli, H., and Hosseini, M. (2022). Assessment of new composites containing polyamide-6 and lead monoxide as shields against ionizing photonic radiation based on computational and experimental methods. *Scientific Reports*, 12:1–15.

Mehrara, R., Malekie, S., Kotahi, S. S., et al. (2021). Introducing a novel low energy gamma ray shield utilizing Polycarbonate Bismuth Oxide composite. *Scientific Reports*, 11:10614.

Mishra, I., Karjodkar, F., Sansare, K., et al. (2018). Diagnostic value of extraoral periapical radiograph in comparison to intraoral periapical radiograph: a cross-sectional, institutional study. *Contemporary Clinical Dentistry*, 9:406–409.

Moafi, M., Geraily, G., Shirazi, A., et al. (2015). Analysis of TLD-100 calibration and Correction factor in different field sizes under low dose conditions irradiated with two systems: Gamma knife 4C and Theratron 780-C. *Frontiers in Biomedical Technologies*, 2:227–236.

More, C., Alsayed, Z., Badawi, M., et al. (2021). Polymeric composite materials for radiation shielding: a review. *Environmental Chemistry Letters*, pages 1–34.

Mortazavi, S., Faghihi, R., Aghamiri, M., et al. (2013). New Challenges in Moving Toward Nano-Sized Lead-Free Radiation Shields. *Medical Physics*, 1:254.

Nair, M. and Nair, U. (2007). Digital and advanced imaging in endodontics: a review. *Journal of endodontics*, 33:1–6.

National Council on Radiation Protection and Measurements (2003). *Radiation protection in dentistry: recommendations of the National Council on Radiation Protection and Measurements*. National Council on Radiation Protection and Measurements, Bethesda.

Navab, M., Hosseini, P., Afarideh, H., et al. (2016). Response of TLD and RPL personal dosimeters in a national intercomparison test program.

Park, S., Lee, J., and Lee, C. (2006). Development of a Korean adult male computational phantom for internal dosimetry calculation. *Radiation protection dosimetry*, 121:257–264.

Pooya, S. and Orouji, T. (2014). Evaluation of effective sources in uncertainty measurements of personal dosimetry by a Harshaw TLD system. *Journal of Biomedical Physics & Engineering*, 4:43.

Qu, X., Li, G., Zhang, Z., et al. (2012). Thyroid shields for radiation dose reduction during cone beam computed tomography scanning for different oral and maxillofacial regions. *European journal of radiology*, 81:e376–e380.

Sadeghi, B., Imani, R. P., Kiani, H., et al. (2025). Comparison of the Measurement Uncertainty of Thermoluminescence Dosimeters (TLD-100 and GR-200) in Clinical Radiotherapy Energies. *Journal of Biomedical Physics and Engineering*.

Shahbazi, L., Sardari, D., Malekie, S., et al. (2026). Evaluation of a flexible thyroid shield in dental panoramic radiography utilizing bismuth oxide silicone rubber composite and Rando phantom. *Scientific Reports*, 16:541.

Srinivasan, K. and Samuel, E. (2017). Evaluation of radiation shielding properties of the polyvinyl alcohol/iron oxide polymer composite. *Journal of medical physics*, 42:273.

Takegami, K., Hayashi, H., Maeda, T., et al. (2023). Thyroid dose reduction shield with the generation of less artifacts used for fast chest CT examination. *Radiation Physics and Chemistry*, 203:110635.

Ufuk, P., Alm, B., Mine, U., et al. (2016). Effect of external magnetic field on the K/K X-ray intensity ratios of TixNi1-x alloys excited by 59.54 and 22.69 keV photons.

Urtekin, E., Perianolu, U., Demir, L., et al. (2020). Investigating photon interaction characteristics of FexNi1-x alloys. *Materials Chemistry and Physics*, 242:122505.

Vollmar, S. and Kalender, W. (2008). Reduction of dose to the female breast in thoracic CT: a comparison of standard-protocol, bismuth-shielded, partial and tube-current-modulated CT examinations. *European radiology*, 18:1674–1682.

Worrall, M., Menhinick, A., and Thomson, D. (2018). The use of a thyroid shield for intraoral anterior oblique occlusal viewsa risk-based approach. *Dentomaxillofacial Radiology*, 47:20170140.

To cite this article:

Malekie, S, Shahbazi, L, Sardari, D, Kashian, S and Kheradmand Saadi, M (2026). Bi_2O_3/silicone rubber composite thyroid shield in periapical radiography: Experimental and Monte Carlo assessment. *Radiation Physics and Engineering*, 7(3), 75–88. doi: 10.22034/rpe.2026.575950.1344

DOI: 10.22034/rpe.2026.575950.1344

To link to this article: https://doi.org/10.22034/rpe.2026.575950.1344